



## Promotion of conductive carbon black loaded $\text{CuFe}_2\text{O}_4$ on the oxidative degradation of phenol by persulfate

Yulu Zhang, Jiping Jia, Nanxin Chang, Yuzeng Zhao\*, Xinjing Meng, Honghua Ge\*

Shanghai Engineering Research Center of Energy-Saving in Heat Exchange Systems, Shanghai Key Laboratory of Materials Protection and Advanced Materials in Electric Power, College of Environmental and Chemical Engineering, Shanghai University of Electric Power, Shanghai 200090, China, emails: zhaoyuzeng@shiep.edu.cn (Y.Z. Zhao), gehonghua@shiep.edu.cn (H.H. Ge), yl\_severus@outlook.com (Y.L. Zhang), m17301781770@163.com (J.P. Jia), c15735640379@yeah.net (N.X. Chang), mengxinjing@shiep.edu.cn (X.J. Meng)

Received 3 March 2022; Accepted 10 June 2022

### ABSTRACT

The development of cheap and efficient catalysts for persulfate activation in advanced oxidation processes based on persulfate is important and promising in the wastewater treatment field. Herein, conductive carbon black loaded  $\text{CuFe}_2\text{O}_4$  (CCB- $\text{CuFe}_2\text{O}_4$ ) had been prepared via a sol-gel method and was used as a catalyst to activate persulfate for the removal of phenol in water. The CCB- $\text{CuFe}_2\text{O}_4$  was characterized by X-ray diffraction, Fourier-transform infrared spectroscopy, Brunauer–Emmett–Teller, and Raman spectroscopy, which confirmed that  $\text{CuFe}_2\text{O}_4$  nucleated on the defect of CCB. The performance of the activation on persulfate was studied by determining the concentration of phenol and chemical oxygen demand of the water. The activity of the catalyst is the highest when the content of  $\text{CuFe}_2\text{O}_4$  in the catalyst is 10%. The removal rate of 100 mg/L phenol reached 100% in 30 min under the optimized operation condition, which was 2.0 g/L CCB- $\text{CuFe}_2\text{O}_4$ , 2.0 mmol/L persulfate (PS) and pH = 11. The factors of effect on the catalysis performance were discussed. CCB- $\text{CuFe}_2\text{O}_4$  can be used in the pH range of 3–11 and the presence of  $\text{HCO}_3^-$  can promote phenol degradation rate. The use of CCB- $\text{CuFe}_2\text{O}_4$  catalyst obviously reduced the dose of PS in the process of phenol oxidation degradation. Furtherly, quenching experiments verified that the most important reactive species in the CCB- $\text{CuFe}_2\text{O}_4$ /PS/phenol system is singlet oxygen ( $^1\text{O}_2$ ).

*Keywords:* Conductive carbon black;  $\text{CuFe}_2\text{O}_4$ ; Persulfate; Phenol; Degradation

### 1. Introduction

Phenolic wastewater is commonly found in coking plants, pharmaceutical plants, and synthetic phenol plants [1,2]. Discharging phenol wastewater directly leads to atmosphere pollution, water pollution, soil pollution, etc. [3,4]. It is reported that the concentration of phenols in drinking water should not exceed one part per billion [5,6]. Therefore, finding efficient methods for phenolic wastewater treatment is important. Many methods have been proposed to remove phenol from aqueous solutions, including adsorption, activated sludge, and advanced oxidation processes (Fenton,

photocatalysis, electrocatalysis, catalytic ozone oxidation, etc.) [7]. In recent years, sulfate radical-based advanced oxidation processes (SR-AOPs) have become a hotspot in wastewater treatment due to their high degradation efficiency and environmentally friendly [8–13].

Persulfate (PS) includes peroxymonosulfate (PMS) and peroxydisulfate (PDS). PDS is more widely used because it is cheaper and more stable in water than PMS [14]. PS can be activated by heat, UV light, bases, and catalysts. The peroxy bonds in PS are broken to generate sulfate radicals to degrade organic pollutants [15]. Activation of PS by heat and UV light has good results but requires more energy

\* Corresponding authors.

consumption [16]. Therefore, the development of efficient catalysts is still an important research direction.

Currently, transition metal oxide catalysts are still the most promising catalysts, and transition metal ions such as cobalt, copper, and manganese are the most effective metal ions for SR-AOPs [17–19]. PS can be activated and generate free radicals by catalysts that compose of transition metal elements [20,21] (Eqs. (1) and (2) [22]). Iron-based catalysts have been extensively studied due to their high performance and cost-effectiveness [19]. Spinel-structured bimetallic ferrites ( $MFe_2O_4$ , where M is a transition metal) have applications in dielectric materials, sensors, and photocatalysis [23]. In addition,  $MFe_2O_4$  is also a catalyst with excellent catalytic performance in SR-AOPs. Magnetic  $MFe_2O_4$  is easy to separate from the aqueous solution and its chemical stability is good, and the amount of metal ion leaching is small, so it is not easy to cause secondary pollution [24]. Li et al. [14] found that  $CuFe_2O_4$  had the best performance in activating PDS among the bimetallic ferrite compounds of Zn, Co, Ni, and Cu. Besides, there have been many reports that  $CuFe_2O_4$  activating PS has been used to degrade water-soluble organic matters [21,25–28]. One study concluded that 0.75 g/L  $CuFe_2O_4$  can activate PDS and degrade 95% of 20 mg/L phenol within 90 min [14]. Recent studies found that PS can also be activated through non-radical pathways by carbon materials [29–33]. The carbon materials acted as an electron mediator to cause electron transfer between PS and organic matters.



At present, most research was aimed at the less concentration (not more than 20 mg/L) of phenol wastewater. At the same time, more PS needs to be added in the catalytic degradation process, which is up to 10–50 times [31,34–36] for the moles of the target organics to be degraded. Therefore, it is necessary to improve the catalytic activity of the catalyst. Single-walled carbon nanotubes can improve the oxidation of PS on phenol degradation due to their excellent conductivity [29]. Conductive carbon black (CCB), which also has excellent conductivity, has the potential to activate PS. In addition, small particle diameter, large specific surface area, and quasi-graphite microstructure [37] make CCB possible to have more catalytic reaction active sites. Moreover, it is low-cost and easy to obtain. Therefore, CCB might be a catalyst with high activity for activating PS. To improve the activity of CCB and reduce the dose of PS in the degradation process,  $CuFe_2O_4$  composed of variable valence Cu and Fe were considered to load on CCB.

In this study,  $CuFe_2O_4$  loaded on CCB (CCB- $CuFe_2O_4$ ) was prepared by a simple sol-gel method, and CCB- $CuFe_2O_4$  was applied in the degradation of high-concentration phenol wastewater by PS. CCB- $CuFe_2O_4$  can effectively activate PS to degrade simulated phenol wastewater. The effects of different degradation conditions on phenol degradation were discussed, including the dose of PS and catalyst, the initial pH, common inorganic anions, and the initial

concentration of phenol. The active species produced in phenol degradation reaction were studied by quenching experiments. The result will provide a valuable reference for the treatment of high concentration of phenol wastewater.

## 2. Materials and methods

### 2.1. Chemicals

CCB was obtained from Cabot Inc., Ltd., America. Nafion PFSA polymer was purchased from DuPont Co., Ltd., USA. Copper nitrate trihydrate ( $Cu(NO_3)_2 \cdot 3H_2O$ ), ferric nitrate nonahydrate ( $Fe(NO_3)_3 \cdot 9H_2O$ ), citric acid monohydrate, potassium iodide (KI), sodium bicarbonate ( $NaHCO_3$ ), potassium persulfate ( $K_2S_2O_8$ ), potassium ferricyanide ( $K_3[Fe(CN)_6]$ ) and sodium carbonate ( $Na_2CO_3$ ) from Sinopharm Chemical Reagent Co., Ltd., (China) were used in the experiments. Phenol, ethanol, tert-butanol, furfuryl alcohol, and 4-aminoantipyrine were purchased from Shanghai Aladdin Chemical Reagent Co., Ltd., China. The water used in the experiments is deionized water.

### 2.2. Synthesis of catalysts

CCB- $CuFe_2O_4$  precursor was synthesized by the sol-gel method. 1.6834 g  $Fe(NO_3)_3 \cdot 9H_2O$  (4 mmol), 0.5034 g  $Cu(NO_3)_2 \cdot 3H_2O$  (2 mmol), and 4.5 g CCB were added into deionized water (40 mL). This mixed solution was magnetically stirred at 60°C for 2 h. Then, 1.3134 g (6 mmol) of citric acid monohydrate was added and continued magnetic stirring at 60°C for 2 h to form a complex gel. Finally, the temperature was increased to 90°C to obtain the CCB- $CuFe_2O_4$  (10%) powdered precursor. CCB- $CuFe_2O_4$  (10%) powder precursor was calcined at 400°C under  $N_2$  atmosphere for 2 h to form CCB- $CuFe_2O_4$  (10%) catalyst. Change the content of  $Fe(NO_3)_3 \cdot 9H_2O$  and  $Cu(NO_3)_2 \cdot 3H_2O$  to obtain CCB- $CuFe_2O_4$  (5%) and CCB- $CuFe_2O_4$  (20%).

### 2.3. Characterization of catalysts

The crystal structure of CCB- $CuFe_2O_4$  was characterized by X-ray diffraction (XRD, D8 ADVANCE, Bruker, Germany) using  $Cu K\alpha$  radiation. The scanning frequency is 10°/min, the step size is 0.02°, and the scanning range is 20°–80°. The Brunauer–Emmett–Teller (BET) specific surface area of CCB- $CuFe_2O_4$  was evaluated from the  $N_2$  adsorption isotherm (BET specific surface area, ASAP 2460, Micromeritics, USA). The samples were pretreated with nitrogen at a degassing temperature of 180°C for 3 h. The infrared spectrum of CCB- $CuFe_2O_4$  was measured by Fourier-transform infrared spectrometer (FTIR, Spectrum Two, PerkinElmer, USA). The test method is Attenuated Total Reflectance Infrared Spectroscopy.

### 2.4. Phenol degradation

The degradation experiment of phenol by CCB- $CuFe_2O_4$  was carried out at room temperature (25°C). 200 mL of 100 mg/L phenol was the target degradation solution, and magnetic stirring was continuously applied during the process.  $K_2S_2O_8$  was added before the reaction started. Water

samples were taken at regular intervals and immediately filtered with a 0.45  $\mu\text{m}$  filter membrane.

#### 2.4.1. Determination of phenol concentration

The concentration of phenol was measured by spectrophotometry [38]. Take a water sample (4 mL) and dilute it 12.5 times to 50 mL. 0.5 mL ammonia-ammonium chloride buffer solution (pH = 10), 1 mL 2% 4-aminoantipyrine and 1 mL 8% potassium ferricyanide were added in sequence. After reacting for 10 min, immediately measure the absorbance at 510 nm with a UV-visible spectrophotometer (UV-visible spectrophotometer, UV-2100, UNICO, USA). The phenol concentration-absorbance standard curve is shown in Fig. 1a. In order to explore whether intermediate products are formed during the degradation process, the degradation experimental samples were also analyzed by direct ultraviolet spectrophotometry. The scanning wavelength range is 200–340 nm.

#### 2.4.2. Chemical oxygen demand measurement

A multi-parameter water quality analyzer (5B-6C (V10), Lianhua, Beijing) was used to measure the chemical oxygen demand (COD) of water samples. The method is based on “Quick Digestion Spectrophotometry (HJ/T399-2007) [39]”. Adopt the high-range dish colorimetric test mode. The reference solution is deionized water.

#### 2.4.3. Determination of $\text{K}_2\text{S}_2\text{O}_8$ concentration

A modified iodometric method was used to test the concentration of potassium persulfate [40]. 0.1 mL water sample, 0.02 g  $\text{NaHCO}_3$ , 0.415 g KI, and 4.9 mL deionized water were mixed. After 20 min of reaction, the absorbance was measured at 352 nm immediately. The  $\text{K}_2\text{S}_2\text{O}_8$  concentration-absorbance standard curve is shown in Fig. 1b.

### 2.5. Reaction mechanism research

#### 2.5.1. Quenching experiment

Add different quenchers before the start of the reaction, the amount added is 50 or 250 times that of PS (the molar

ratio). The other steps are the same as the phenol degradation experiment in 2.4.

#### 2.5.2. Raman spectrum

Raman spectroscopy (Raman Spectrum, LabRAM, Horiba Jobin Yvon, France) was used to measure the Raman spectra of CCB and CCB- $\text{CuFe}_2\text{O}_4$ . The tested laser wavelength was 532 nm and the power was 2.58 mW.

#### 2.5.3. Linear sweep voltammetry

Shanghai Chenhua CHI660E electrochemical workstation was used to perform the linear sweep voltammetry test. The electrolyte was 10 mmol/L phosphate buffer solution. 0.5 mL of ethanol, 10  $\mu\text{L}$  of Nafion solution, and 3 mg of catalyst were put together into a small glass bottle. Ultrasound for 15 min at 25°C. Drop 10  $\mu\text{L}$  solution on the 3 mm diameter glassy carbon electrode, which is the working electrode. The counter electrode and reference electrode were Pt electrode (1 cm  $\times$  1 cm) and Ag-AgCl electrode, respectively. The test potential range is 0.2–1.6 V, and the scanning speed is 20 mV/s.

## 3. Results and conclusions

### 3.1. Catalyst preparation and characterization

The prepared catalyst was black powder. The crystal structures of CCB and  $\text{CuFe}_2\text{O}_4$  were studied by XRD (Fig. 2a). The peaks at 25.22° and 43.70° were the characteristic peaks of CCB. (2 2 0), (3 1 1), (4 0 0), (5 1 1) and (4 4 0) planes correspond to the peaks at 30.05°, 35.67°, 43.39°, 57.20°, and 62.66°, which were the characteristic peaks of spinel  $\text{CuFe}_2\text{O}_4$  [41]. Meanwhile, the sample of CCB- $\text{CuFe}_2\text{O}_4$  (10%) was also characterized. The XRD pattern of CCB- $\text{CuFe}_2\text{O}_4$  (10%) showed both CCB and  $\text{CuFe}_2\text{O}_4$  crystal structure, indicating that CCB- $\text{CuFe}_2\text{O}_4$  (10%) was successfully synthesized by the sol-gel method. The peak at 53.47° corresponded to the diffraction peak of the (4 2 1) crystal plane of  $\text{Fe}_2\text{O}_3$ . The intensity of this peak was obviously smaller than the characteristic peak of  $\text{CuFe}_2\text{O}_4$ , which might be due to the excessive amount of Fe source in the raw material, which led to the formation of a small amount of  $\text{Fe}_2\text{O}_3$  [24]. In

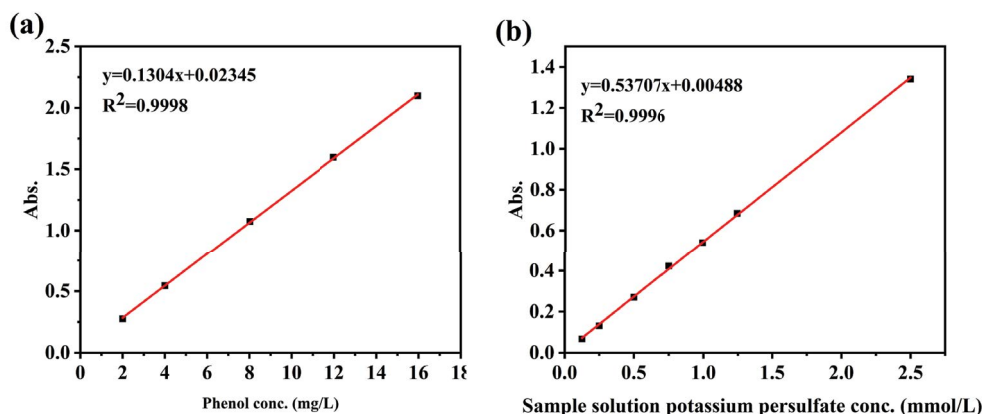


Fig. 1. (a) Phenol absorbance standard curve and (b) potassium persulfate absorbance standard curve.

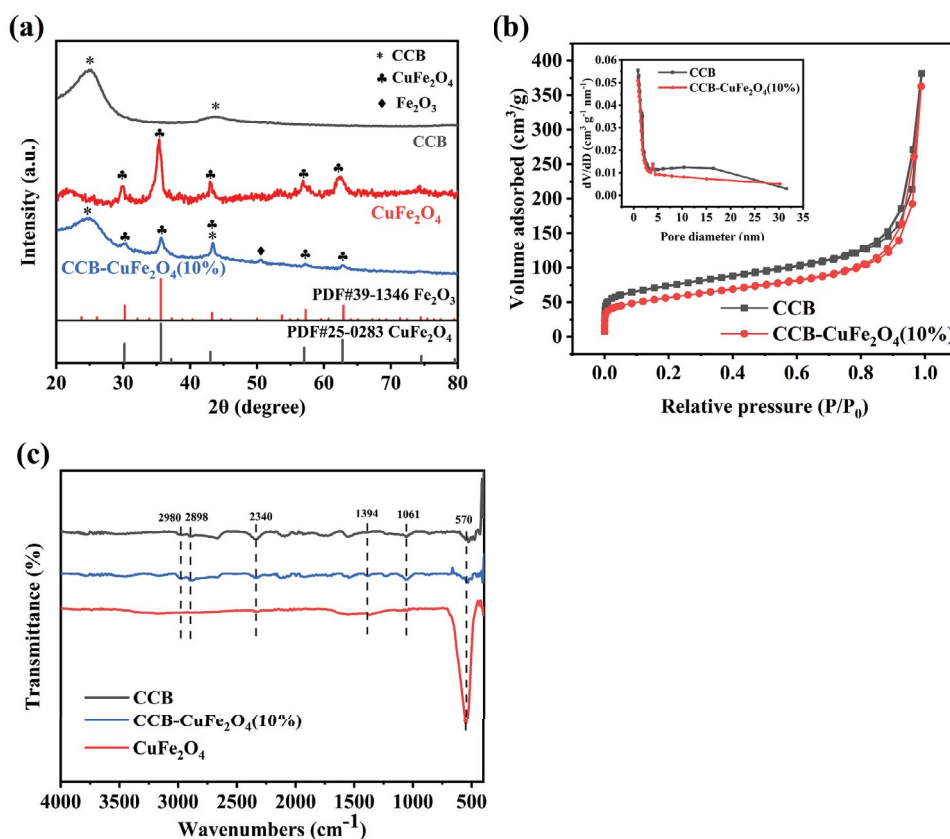


Fig. 2. (a) XRD image, (b)  $N_2$  adsorption–desorption isotherm and (c) FTIR spectra.

addition, the peak width of the characteristic peaks belonging to  $CuFe_2O_4$  increased slightly, while the peak width of the carrier CCB was almost unchanged, which indicated that the grain size of  $CuFe_2O_4$  decreased after being dispersed on the CCB. According to the full width at the half-maximum of the diffraction peak, the grain size was calculated by the Scherrer equation [42] [Eq. (3)]. The average size of  $CuFe_2O_4$  crystals was 12.7 nm. However, the average size of  $CuFe_2O_4$  crystals (11.3 nm) in CCB- $CuFe_2O_4$  (10%) was reduced (Table 1). The results showed that the growth of  $CuFe_2O_4$  on CCB improves the dispersibility of  $CuFe_2O_4$ .

$$D_{hkl} = \frac{K\lambda}{\beta_{hkl} \cos\theta_{hkl}} \quad (3)$$

where  $D_{hkl}$  is the crystallite size perpendicular to the normal line of the (h k l) plane,  $K$  is a constant,  $\lambda$  is the X-ray wavelength,  $\beta_{hkl}$  is the full width at half maximum of the (h k l) diffraction peak,  $\theta_{hkl}$  is the Bragg angle of the (h k l) peak.

The catalyst requires a suitable specific surface area [43], which could be measured by the BET method. Before and after  $CuFe_2O_4$  has been loaded on CCB, their adsorption equilibrium isotherms were the type IV adsorption equilibrium isotherm (Fig. 2b). CCB was mainly microporous and mesoporous structures. After  $CuFe_2O_4$  had been loaded on CCB, the specific surface area of the catalyst decreased, the pore volume was almost unchanged, and the pore size increased slightly.

Table 1  
Structural characteristics of the sample

Sample	$S_{BET}$ ( $m^2/g$ )	Pore volume ( $cm^3/g$ )	Pore size (nm)
CCB	249.68	0.54	6.88
CCB- $CuFe_2O_4$ (10%)	193.51	0.53	7.62

Fig. 2c shows the FTIR spectra of CCB,  $CuFe_2O_4$ , and CCB- $CuFe_2O_4$  (10%). The peak at  $1,061\text{ cm}^{-1}$  represented the stretching vibration of C–O [44]. The peak at  $1,394\text{ cm}^{-1}$  was attributable to the vibration of C–OH, and surface hydroxyl groups might be catalytically converted into active oxygen species [45]. The peak at  $2,340\text{ cm}^{-1}$  represented the stretching vibration of O=C=O [46]. The peaks at  $2,898$  and  $2,980\text{ cm}^{-1}$  represented the vibration of C–H [47]. After  $CuFe_2O_4$  was modified, the types of functional groups did not change much. In the FTIR spectra of CCB- $CuFe_2O_4$  (10%), due to the low content of  $CuFe_2O_4$ , the peaks at  $570$  and  $480\text{ cm}^{-1}$  represent Fe–O and Cu–O vibration [21] could not be observed.

### 3.2. Performance of the catalyst

The phenol removal rate and the change of  $K_2S_2O_8$  concentration were used to analyze the activation of CCB- $CuFe_2O_4$  on PDS in different systems. Phenol hardly

degraded in the presence of  $K_2S_2O_8$  alone. When CCB existed alone, the removal rate of phenol is about 47%. The first 5 min were the adsorption of phenol, and then the adsorption equilibrium was reached. When CCB- $CuFe_2O_4$  (10%) existed alone, the removal rate of phenol (about 30%) is reduced, because the specific surface area of CCB- $CuFe_2O_4$  (10%) was smaller than that of CCB. However, after adding both  $K_2S_2O_8$  and CCB or CCB- $CuFe_2O_4$  (10%), the concentration of phenol decreased rapidly. Both CCB and CCB- $CuFe_2O_4$  (10%) could effectively activate  $K_2S_2O_8$ , and the activity of CCB- $CuFe_2O_4$  (10%) was higher. The better catalytic activity of CCB- $CuFe_2O_4$  (10%) is attributed to the spinel-structured  $CuFe_2O_4$  containing transition metal elements [23,24]. Fig. 3b shows the change of  $K_2S_2O_8$  concentration in different systems. When only phenol was present, the concentration of  $K_2S_2O_8$  will not change, that was,  $K_2S_2O_8$  had not been activated. When only CCB or CCB- $CuFe_2O_4$  (10%) existed, the concentration of  $K_2S_2O_8$  decreased. However, when phenol and CCB or CCB- $CuFe_2O_4$  (10%) were added at the same time, the  $K_2S_2O_8$  concentration decreased more, which proved that  $K_2S_2O_8$  was activated and the system was selective for the degradation of phenol. The high electron cloud density in phenol might be the reason why  $K_2S_2O_8$  was easier to activate. The reaction stoichiometric efficiency (RSE) of PS for the degradation of phenol by CCB- $CuFe_2O_4$  (10%) can be calculated according to the following equation [Eq. (4)] [48]:

$$\delta = \frac{\Delta C_{\text{Phenol}}}{\Delta C_{\text{PDS}}} \quad (4)$$

where  $\Delta C_{\text{phenol}}$  and  $\Delta C_{\text{PDS}}$  represent the concentration of phenol degraded and the corresponding concentration of PS consumed, respectively.

Calculations based on the phenol consumed and PS consumed in the CCB/PS/phenol system and the CCB- $CuFe_2O_4$ /PS/phenol system in Fig. 3b yielded  $\delta(\text{CCB}) = 66.96\%$  and  $\delta(\text{CCB-}CuFe_2O_4) = 52.25\%$ . Table 2 showed the RSE of PS for the degradation of phenol with different catalyst activations of PS. Our catalysts have a higher RSE for PS.

The CCB was modified with  $CuFe_2O_4$  so that the mass of  $CuFe_2O_4$  accounted for 0%, 5%, 10%, and 20% of the total

Table 2  
RSE for PS in catalyst/PS/phenol systems reported in different studies

Phenol conc. (mg/L)	Sample	RSE of PS (%)	References
200	Biochar	about 20	[49]
20	CuO	45–50	[50]
10	$FeS_2/Fe^0$	60.43	[51]
100	CCB- $CuFe_2O_4$	52.25	This work

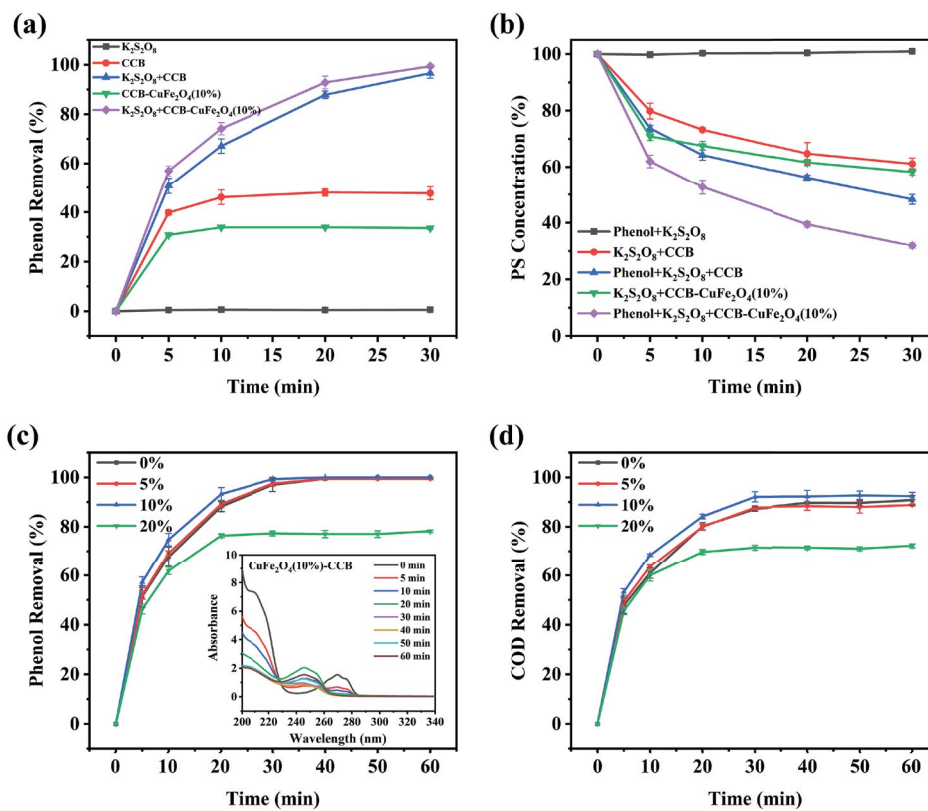


Fig. 3. (a) Degradation of phenol, (b) consumption of  $K_2S_2O_8$  under different systems, and (c) phenol removal rate, (d) COD removal rate in the CCB- $CuFe_2O_4$ /PS/phenol system when  $CuFe_2O_4$  modification amount is different. The inset figure in (c) is the UV spectrum of CCB- $CuFe_2O_4$  (10%) degrading phenol. Experimental conditions: [phenol] = 100 mg/L; [catalyst] = 2 g/L; [PS] = 3 mmol/L.

mass, and the degradation experiment was carried out under the same conditions. Fig. 3c displays the ability of different loadings of  $\text{CuFe}_2\text{O}_4$  to degrade phenol. When the  $\text{CuFe}_2\text{O}_4$  modification amount was 10%, the performance of CCB- $\text{CuFe}_2\text{O}_4$  was better than single CCB and single  $\text{CuFe}_2\text{O}_4$ . The COD removal rate in Fig. 3d shows the same regulation. When the modification amount of  $\text{CuFe}_2\text{O}_4$  was 20%, the catalytic performance decreased rapidly, probably due to the occupation of too many catalytic reaction sites on the CCB. A moderate amount of CCB improved the dispersibility of  $\text{CuFe}_2\text{O}_4$  and make the grains smaller, and also increases the specific surface area of the catalyst. The increase of specific surface area enables  $\text{CuFe}_2\text{O}_4$  per unit mass to contact with more  $\text{K}_2\text{S}_2\text{O}_8$  and catalyze the reaction, that is, the catalytic performance of  $\text{CuFe}_2\text{O}_4$  per unit mass is improved. The inset in Fig. 3c shows the UV spectrum of the catalyst with a loading of 10% when degrading phenol. Before the reaction, there were obvious absorption peaks at 210 and 270 nm, both of which were absorption peaks of phenol. As the degradation progresses, the absorption peaks at 210 and 270 nm decreased rapidly, which meant that phenol had been degraded. Meanwhile, a new absorption peak representing benzoquinone [36] was generated at about 245 nm.

### 3.3. Effect of degradation conditions

#### 3.3.1. Effect of PDS doses

A series of tests were performed to study the effect of PDS doses on phenol degradation (Fig. 4a). The result indicated that when  $\text{K}_2\text{S}_2\text{O}_8$  was not added, it was only the physical adsorption process of CCB- $\text{CuFe}_2\text{O}_4$  (10%). The addition of  $\text{K}_2\text{S}_2\text{O}_8$  could effectively activate CCB- $\text{CuFe}_2\text{O}_4$  (10%) to degrade phenol. When the concentration of  $\text{K}_2\text{S}_2\text{O}_8$  was 1 mmol/L, the reaction stopped after 30 min, because  $\text{K}_2\text{S}_2\text{O}_8$  was consumed. By increasing the amount of  $\text{K}_2\text{S}_2\text{O}_8$  to

2 mmol/L, the removal rate of phenol reached the maximum. At this time, the reaction rate constant was  $0.02891 \text{ min}^{-1}$  (Fig. 4b). Excessive PS could undergo a self-coupling reaction with  $\text{SO}_4^-$  [52]. But, as the concentration of  $\text{K}_2\text{S}_2\text{O}_8$  continues to increase, the efficiency of phenol degradation hardly increased, this may be because excess PDS leads to self-quenching of  $\text{SO}_4^-$  or the reaction of  $\text{SO}_4^-$  and  $\text{S}_2\text{O}_8^{2-}$  to form the less reactive  $\text{S}_2\text{O}_8^-$  [19].

#### 3.3.2. Effect of catalyst doses

Fig. 5a illustrated the effect of catalyst doses on phenol degradation. Phenol could not be oxidized in the PS-only systems. With the increase of CCB- $\text{CuFe}_2\text{O}_4$  (10%) doses, the degradation efficiency of phenol increased significantly, and the relationship between the two was positively correlated. At the same time, the reaction rate constant increased from  $0.02891 \text{ min}^{-1}$  ([catalyst] = 1 g/L) to  $0.08087 \text{ min}^{-1}$  ([catalyst] = 2.5 g/L), as shown in Fig. 5b. This conclusion was attributed to: (i) The first 5 min were mainly for adsorption. As the catalyst doses increase, more and more phenol and  $\text{K}_2\text{S}_2\text{O}_8$  were adsorbed on the catalyst, which was beneficial to the subsequent catalytic reaction [26]; (ii) More catalysts had more active sites to participate in the catalytic reaction.

#### 3.3.3. Effect of initial pH

It is generally accepted that the initial pH of the solution will affect the properties of phenol or the formation of active free radicals, and it will also change the performance of the catalyst. In order to study the effect of initial pH on phenol degradation,  $\text{H}_2\text{SO}_4$  (0.2 mol/L) and  $\text{NaOH}$  (0.2 mol/L) were used to adjust the initial pH to 3–11 for phenol degradation. As could be seen, the change in initial pH not affected the degradation of phenol to a large extent (Fig. 6a). Phenol degradation was promoted when the initial pH = 3, probably due to the positive surface charge of  $\text{CuFe}_2\text{O}_4$  after adsorption

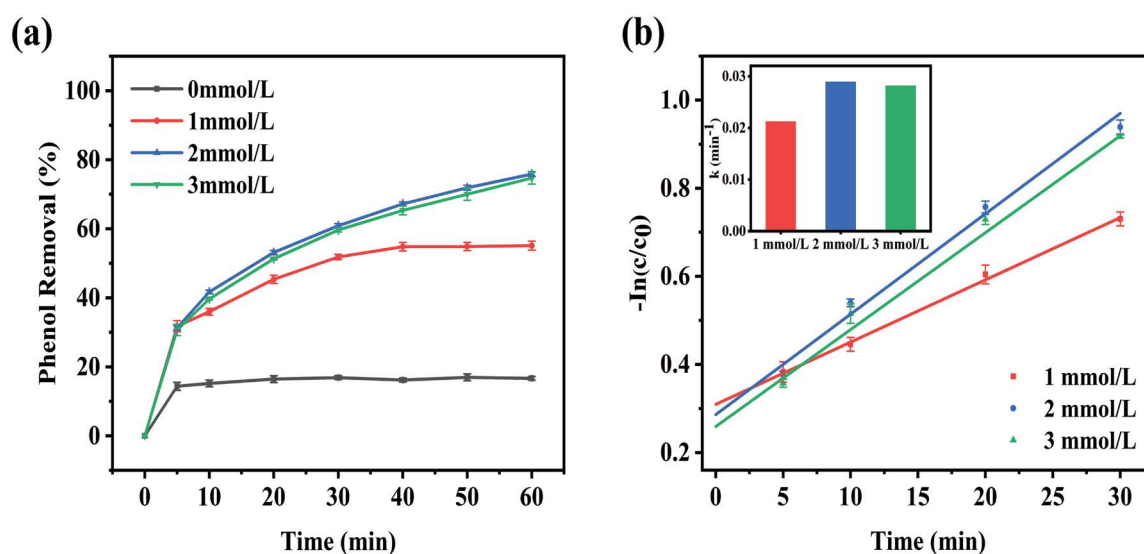


Fig. 4. (a) Effect of PDS doses on phenol degradation and (b) kinetic fitting of phenol degradation with different PDS doses. The inset figure in (b) is the reaction rate constants obtained after kinetic fitting. Experimental conditions: [phenol] = 100 mg/L; [catalyst] = 2 g/L.

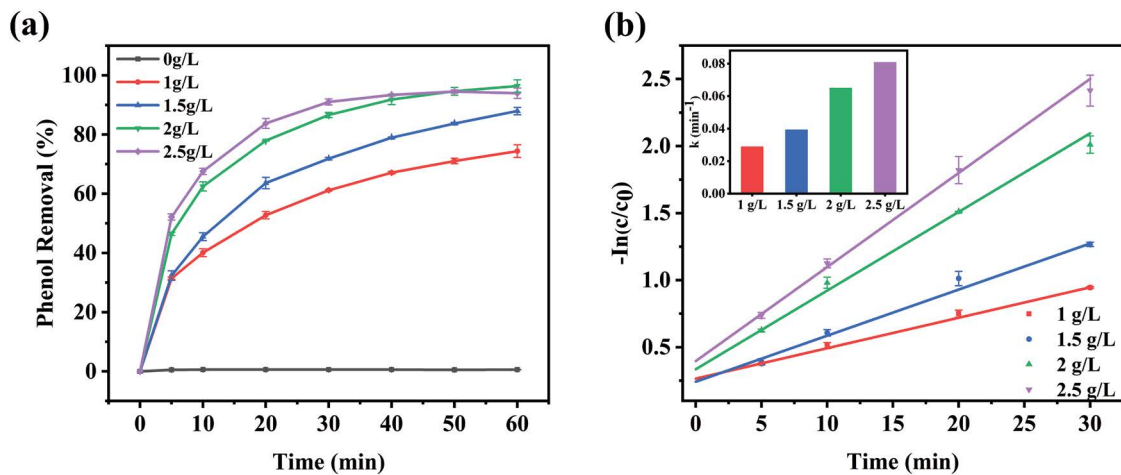


Fig. 5. (a) Effect of catalyst doses on phenol degradation and (b) kinetic fitting of phenol degradation with different catalyst doses. The inset figure in (b) is the reaction rate constants obtained after kinetic fitting. Experimental conditions: [phenol] = 100 mg/L; [PS] = 2 mmol/L.

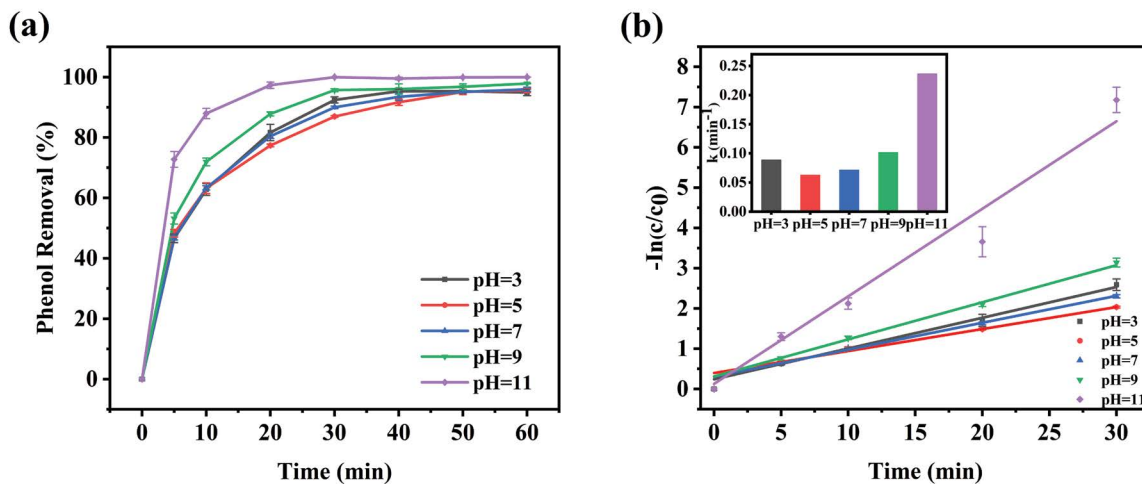


Fig. 6. (a) Effect of initial pH on phenol degradation and (b) kinetic fitting of phenol degradation with different initial pH. The inset figure in (b) is the reaction rate constants obtained after kinetic fitting. Experimental conditions: [phenol] = 100 mg/L; [catalyst] = 2 g/L; [PS] = 2 mmol/L.

of  $H^+$ , which promoted contact between the catalyst and  $S_2O_8^{2-}$  through electrostatic attraction, producing reactive material [24]. It was worth noting that the degradation rate of phenol reaches a maximum when the initial pH = 11, which may be due to the activation of persulfate by base.

### 3.3.4. Common inorganic ions in water

The water to be treated often contains a variety of inorganic anions ( $HCO_3^-$ ,  $Cl^-$ ,  $SO_4^{2-}$ ,  $NO_3^-$ , etc.), and their presence may interfere with the degradation experiment [53]. Under the same degradation conditions, we added different anions (5 mmol/L) to explore their effects on the CCB- $CuFe_2O_4$ /PS/phenol degradation system (Fig. 7a). Studies had shown that the presence of  $Cl^-$  has inhibitory and scavenging effects on the degradation system, which was attributed to the consumption of  $OH$  and  $SO_4^{\cdot -}$  in the reaction system

and the generation of  $Cl$  [Eqs. (5)–(7)] [54]. In this study, the addition of  $Cl^-$  slightly promoted the degradation of phenol, which may be due to the oxidative ability of the  $HOCl/Cl_2$  system (Eqs. (8) and (9)) [55]. The addition of  $SO_4^{2-}$  did not affect the final phenol removal rate. The addition of  $HCO_3^-$  promoted the degradation of phenol, which may be attributed to the increase of solution pH. Fig. 7b showed that when  $HCO_3^-$  was present in the system, the pH of the solution was about 4 higher than that of the other systems. The addition of  $NO_3^-$  reduced the reaction rate slightly, the possible reason is that  $NO_3^-$  would be adsorbed in the heterogeneous catalyst [46], thereby reducing the catalytic performance of the catalyst. In general,  $Cl^-$ ,  $SO_4^{2-}$ ,  $NO_3^-$  and other common anions that could react with free radicals have little effect on the CCB- $CuFe_2O_4$ /PS/phenol degradation system. However,  $HCO_3^-$  could promote the degradation reaction due to its characteristic of being hydrolyzed to alkalinity.

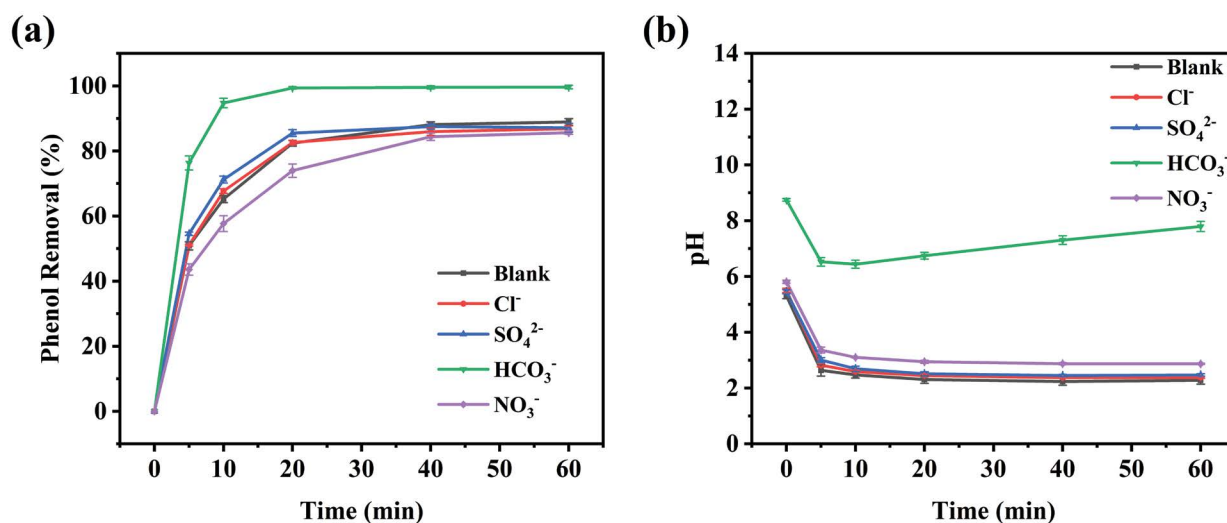
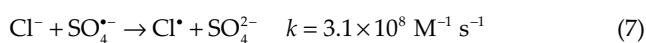
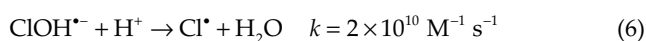
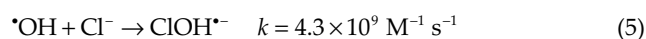


Fig. 7. (a) Effect of different anions on the degradation of phenol and (b) change of pH value of the solution caused by different anions. Experimental conditions: [phenol] = 100 mg/L; [catalyst] = 2 g/L; [PS] = 2 mmol/L.



### 3.3.5. Initial phenol concentration

The effect of initial phenol concentration is shown in Fig. 8. As could be seen, 20 and 60 mg/L phenol could be completely degraded within 10 and 20 min, respectively. When the initial phenol concentration was increased to 100 mg/L, the removal rate of phenol could reach 95% in 60 min. So, as the concentration of phenol increased, the degradation rate of phenol became slower.

By studying the effects of different operating parameters on phenol degradation, the optimal conditions for 100 mg/L phenol degradation were obtained. The removal rate of 100 mg/L phenol reached 100% in 30 min under optimized operation condition, which was 2.0 g/L CCB-CuFe<sub>2</sub>O<sub>4</sub>, 2.0 mmol/L PS and pH = 11. Table 3 listed the catalytic activity when different catalysts activate PS to degrade phenol. It was found that CCB-CuFe<sub>2</sub>O<sub>4</sub> (10%) achieves less PS addition during phenol degradation performance.

### 3.4. Reaction mechanism

It is generally believed that the reactive species produced by activating persulfate are  $\cdot\text{OH}$ ,  $\text{SO}_4^{\cdot-}$ ,  $\text{O}_2^{\cdot-}$ , and  $^1\text{O}_2$ . In order to study the reactive species in the CCB-CuFe<sub>2</sub>O<sub>4</sub>/

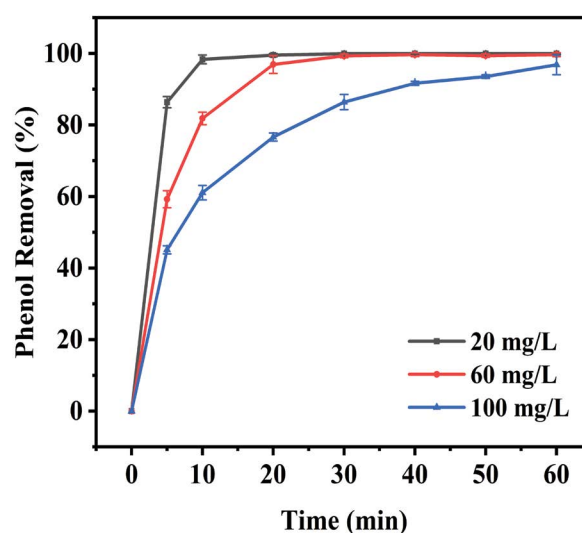


Fig. 8. Effect of different initial concentrations of phenol on the degradation of phenol. Experimental conditions: [catalyst] = 2 g/L; [PS] = 2 mmol/L.

K<sub>2</sub>S<sub>2</sub>O<sub>8</sub>/phenol system, a series of quenchers were added to the catalytic system. The second-order rate constant of tert-butanol (TBA) and OH ( $3.8\text{--}7.6 \times 10^8 \text{ M}^{-1} \text{ s}^{-1}$ ) is much larger than that of TBA and SO<sub>4</sub><sup>·-</sup> ( $4.4\text{--}9.1 \times 10^5 \text{ M}^{-1} \text{ s}^{-1}$ ) [34], so the presence of OH could be determined. The second-order rate constants of ethanol (EtOH) with OH and SO<sub>4</sub><sup>·-</sup> are  $1.2\text{--}2.8 \times 10^9 \text{ M}^{-1} \text{ s}^{-1}$  and  $1.6\text{--}7.7 \times 10^7 \text{ M}^{-1} \text{ s}^{-1}$  [57], respectively, and are often used as OH and SO<sub>4</sub><sup>·-</sup> quencher. Na<sub>2</sub>CO<sub>3</sub> can act as the quencher for O<sub>2</sub><sup>·-</sup> and  $^1\text{O}_2$  [58]. As presented in Fig. 9a, the addition of TBA and EtOH has no significant effect on phenol degradation, which proves that OH and SO<sub>4</sub><sup>·-</sup> were not the main reactive species in the system. The quenching effect of adding TBA, which only reacted with OH, was better than that of EtOH, because EtOH is hydrophilic

Table 3  
Catalytic activity of different catalysts to activate PS to degrade phenol reported in the literature

Phenol conc. (mg/L)	Catalyst	Catalyst:phenol (mass ratio)	PS:phenol (the molar ratio)	Reaction time (min)	Phenol degradation	References
19.74	CuFe <sub>2</sub> O <sub>4</sub>	0.03	4.76	90	97%	[14]
9.4	Single-walled carbon nanotubes	0.09	10	60	100%	[30]
9.4	Fe-doped g-C <sub>3</sub> N <sub>4</sub>	0.01	50	20	95%	[32]
9.4	CuO <sub>x</sub> @Co-LDH	0.03	50	40	100%	[35]
20	Cubic mesoporous carbons	0.10	30.55	20	100%	[36]
20	N-doped graphene aerogel	0.07	34.78	60	100%	[37]
20	Fe@porous carbon	0.07	5.22	120	100%	[56]
100	CCB-CuFe <sub>2</sub> O <sub>4</sub>	0.05	1.88	30	100%	This work

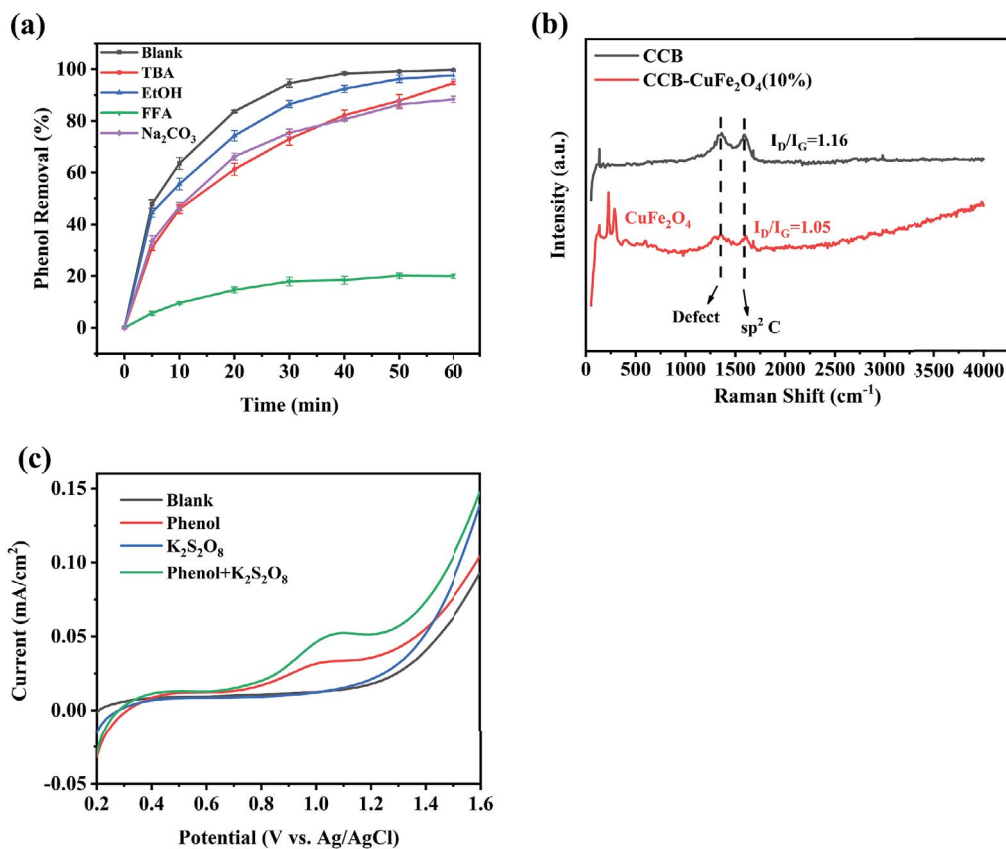


Fig. 9. (a) Degradation of phenol with and without oxidant scavenger CCB-CuFe<sub>2</sub>O<sub>4</sub>/PS system (Test conditions: [phenol] = 100 mg/L; [catalyst] = 2 g/L; [PS] = 2 mmol/L; [TBA] = 500 mmol/L; [EtOH] = 500 mmol/L; [Na<sub>2</sub>CO<sub>3</sub>] = 100 mmol/L; [FFA] = 100 mmol/L), (b) Raman spectra of CCB and CCB-CuFe<sub>2</sub>O<sub>4</sub> and (c) linear sweep voltammogram in the presence of PS and phenol (Test conditions: [phenol] = 100 mg/L; [PS] = 2 mmol/L; pH = 7.0 (10 mmol/L phosphate buffer solution)).

and easy to disperse in the solution. While TBA is hydrophobic, easy to adsorb on the surface of the catalyst, and can quench some free radicals on the surface of the catalyst [56]. Besides, after adding Na<sub>2</sub>CO<sub>3</sub>, the removal rate of phenol decreased slightly. The FFA obviously suppressed

the removal rate of phenol. Combined with the quenching results of FFA and TBA, it was concluded that there was more <sup>1</sup>O<sub>2</sub> in the reaction system. In short, the active species in the CCB-CuFe<sub>2</sub>O<sub>4</sub>/PS/phenol degradation system were mainly <sup>1</sup>O<sub>2</sub>, some SO<sub>4</sub><sup>-</sup>, and a small content of OH and O<sub>2</sub><sup>-</sup>.

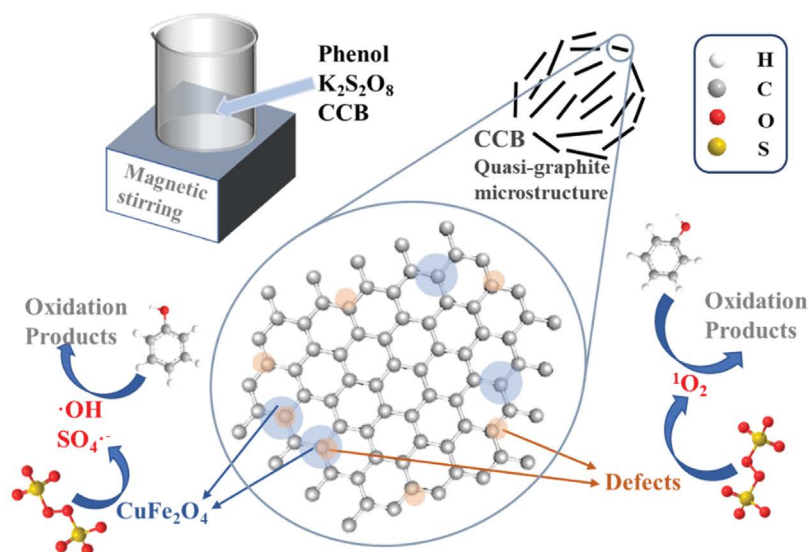


Fig. 10. Reaction mechanism of CCB-CuFe<sub>2</sub>O<sub>4</sub>/PS/phenol degradation system.

SO<sub>4</sub><sup>·-</sup> was usually produced by transition metal activation of PS [60]. Studies had shown that <sup>1</sup>O<sub>2</sub> could be produced at catalyst defects and C=O [32].

The location of CuFe<sub>2</sub>O<sub>4</sub> growth was verified by the Raman results (Fig. 9b). For CCB, obvious D and G bands were observed at 1,350 and 1,590 cm<sup>-1</sup>, respectively. The D band was caused by defects, and the G band was caused by sp<sup>2</sup> hybridized carbon [36]. The D and G bands in the Raman spectrum of CCB-CuFe<sub>2</sub>O<sub>4</sub> decreased at the same time, which indicated that the growth position of CuFe<sub>2</sub>O<sub>4</sub> was the CCB defect and the sp<sup>2</sup> hybrid carbon around the defect, and CuFe<sub>2</sub>O<sub>4</sub> grew uniformly. After CuFe<sub>2</sub>O<sub>4</sub> modification, I<sub>D</sub>/I<sub>G</sub> decreased from 1.16 to 1.05, proving that the defects of the catalyst were reduced. However, the activity of the catalysts after modification by CuFe<sub>2</sub>O<sub>4</sub> increased, because CuFe<sub>2</sub>O<sub>4</sub> could activate PS to generate free radicals through Fe and Cu valence changes [61–63], and this part of the active species contributed more than the active species generated by the defects occupied by CuFe<sub>2</sub>O<sub>4</sub>.

CCB had a certain specific surface area and a suitable porous structure, which was conducive to the progress of the catalytic process [64]. In addition, the excellent conductivity of CCB could accelerate the transfer of electrons. Studies had proved that the carbon material catalyst acts as an electron mediator, which greatly increases the transfer speed of electrons between PS and phenol [29]. Fig. 9c displays that there is a broad oxidation peak at 0.8–1.2 V in the presence of phenol, and the current response increased in the presence of K<sub>2</sub>S<sub>2</sub>O<sub>8</sub>. In particular, when phenol and K<sub>2</sub>S<sub>2</sub>O<sub>8</sub> existed at the same time, the current response increased more, indicating that CCB-CuFe<sub>2</sub>O<sub>4</sub> in the CCB-CuFe<sub>2</sub>O<sub>4</sub>/PS/phenol degradation system could act as an electron mediator to promote the degradation of phenol.

As discussed above, the CCB-CuFe<sub>2</sub>O<sub>4</sub> heterogeneous catalytic activation process of K<sub>2</sub>S<sub>2</sub>O<sub>8</sub> with free radical mechanism and non-radical mechanism coexisting was speculated. As shown in Fig. 10, free radical mechanism: CuFe<sub>2</sub>O<sub>4</sub> activated K<sub>2</sub>S<sub>2</sub>O<sub>8</sub> to generate free radicals to oxidize phenol

[42]. Non-radical mechanism: PS was activated at the CCB defect and C=O on the surface of CCB to generate <sup>1</sup>O<sub>2</sub> [32,65]. The reactive site that contributed the most to the degradation of phenol was the defect site of CCB.

#### 4. Conclusions

In this work, CCB-CuFe<sub>2</sub>O<sub>4</sub> was prepared by a simple sol-gel method to activate PS to degrade simulated phenol wastewater. The optimal operating parameters for the degradation of 100 mg/L phenol were obtained. When the dose of CCB-CuFe<sub>2</sub>O<sub>4</sub> was 2.0 g/L, the dose of PS was 2.0 mmol/L, and initial pH = 11, the phenol removal rate reached 100% after 30 min. Cl<sup>-</sup>, SO<sub>4</sub><sup>2-</sup>, NO<sub>3</sub><sup>-</sup> had almost no effect on the degradation of phenol, and HCO<sub>3</sub><sup>-</sup> could increase the pH value of the solution and promote the degradation of phenol. Infrared spectroscopy showed the existence of C=O; Raman spectroscopy confirmed the existence of defects in CCB and the formation of CuFe<sub>2</sub>O<sub>4</sub> at the defects of CCB. The quenching experiment proved that the main reactive species in the reaction system is <sup>1</sup>O<sub>2</sub>, and <sup>1</sup>O<sub>2</sub> was produced at the defects and C=O on the surface of CCB. Besides, CuFe<sub>2</sub>O<sub>4</sub> grown on CCB had a smaller particle size and more reactive sites to improve the performance of the catalyst. LSV showed that the electron transfer speed was accelerated in CCB-CuFe<sub>2</sub>O<sub>4</sub>/PS/phenol system. Free radical mechanism and non-radical mechanism coexist in the process of CCB-CuFe<sub>2</sub>O<sub>4</sub> heterogeneous catalytic activation of K<sub>2</sub>S<sub>2</sub>O<sub>8</sub>. The results showed that CCB-CuFe<sub>2</sub>O<sub>4</sub> achieved a smaller dose of PS in the process of catalytic activation of PS, which provided new insights for the development of activated PS catalysts.

#### Acknowledgements

This work is financially supported by Science and Technology Commission of Shanghai (19DZ2271100) and Natural Science Foundation of Shanghai (Grant Nos. 20ZR1421500).

## References

- [1] Y. Ghaffari, N.K. Gupta, J. Bae, K.S. Kim, Heterogeneous catalytic performance and stability of iron-loaded ZSM-5, zeolite-A, and silica for phenol degradation: a microscopic and spectroscopic approach, *Catalysts*, 9 (2019) 859, doi: 10.3390/catal9100859.
- [2] C.M. Chen, X.Y. Yao, Q.X. Li, Q.H. Wang, J.H. Liang, S.M. Zhang, J. Meng, Z.Y. Liu, J.M. Deng, B.A. Yoza, Turf soil enhances treatment efficiency and performance of phenolic wastewater in an up-flow anaerobic sludge blanket reactor, *Chemosphere*, 204 (2018) 227–234.
- [3] S.Q. Liu, Z.C. Zhang, F. Huang, Y.Z. Liu, L. Feng, J. Jiang, L.Q. Zhang, F. Qi, C. Liu, Carbonized polyaniline activated peroxymonosulfate (PMS) for phenol degradation: role of PMS adsorption and singlet oxygen generation, *Appl. Catal., B*, 286 (2021) 119921, doi: 10.1016/j.apcatb.2021.119921.
- [4] D. Amado-Piña, G. Roa-Morales, C. Barrera-Díaz, P. Balderas-Hernandez, R. Romero, E. Martín del Campo, R. Natividad, Synergic effect of ozonation and electrochemical methods on oxidation and toxicity reduction: phenol degradation, *Fuel*, 198 (2017) 82–90.
- [5] M. Alshabib, S.A. Onaizi, A review on phenolic wastewater remediation using homogeneous and heterogeneous enzymatic processes: current status and potential challenges, *Sep. Purif. Technol.*, 219 (2019) 186–207.
- [6] M.L. Han, J. Zhang, W. Chu, G.F. Zhou, J.H. Chen, Surface-modified sewage sludge-derived carbonaceous catalyst as a persulfate activator for phenol degradation, *Int. J. Environ. Res. Public Health*, 17 (2020) 3286, doi: 10.3390/ijerph17093286.
- [7] W.H. Saputera, A.S. Putri, A.A. Esmailpour, D. Sasongko, V. Suendo, R.R. Mukti, Technology advances in phenol removals: current progress and future perspectives, *Catalysts*, 11 (2021) 998, doi: 10.3390/catal11080998.
- [8] J.L. Wang, S.Z. Wang, Reactive species in advanced oxidation processes: formation, identification and reaction mechanism, *Chem. Eng. J.*, 401 (2020) 126158, doi: 10.1016/j.cej.2020.126158.
- [9] H.Z. Wang, W.Q. Guo, B.H. Liu, Q.L. Wu, H.C. Luo, Q. Zhao, Q.S. Si, F. Sseguya, N.Q. Ren, Edge-nitrogenated biochar for efficient peroxydisulfate activation: an electron transfer mechanism, *Water Res.*, 160 (2019) 405–414.
- [10] H.J. Zhou, D.X. Lu, S.Q. Fang, C. Liu, Y.C. Chen, Y.Y. Hu, Q.J. Luo, Prompting direct single electron transfer to produce non-radical  $^1\text{O}_2/\text{H}^*$  by electro-activating peroxydisulfate process with core-shell cathode, *J. Environ. Manage.*, 287 (2021) 112294, doi: 10.1016/j.jenvman.2021.112294.
- [11] P. Ye, D.M. Wu, M.Y. Wang, Y. Wei, A.H. Xu, X.X. Li, Coating magnetic  $\text{CuFe}_2\text{O}_4$  nanoparticles with OMS-2 for enhanced degradation of organic pollutants via peroxymonosulfate activation, *Appl. Surf. Sci.*, 428 (2018) 131–139.
- [12] Q.X. Zhao, Q.M. Mao, Y.Y. Zhou, J.H. Wei, X.C. Liu, J.Y. Yang, L. Luo, J.C. Zhang, H. Chen, H.B. Chen, L. Tang, Metal-free carbon materials-catalyzed sulfate radical-based advanced oxidation processes: a review on heterogeneous catalysts and applications, *Chemosphere*, 189 (2017) 224–238.
- [13] J.F. Yu, H.P. Feng, L. Tang, Y. Pang, G.M. Zeng, Y. Lu, H.R. Dong, J.J. Wang, Y.N. Liu, C.Y. Feng, J.J. Wang, B. Peng, S.J. Ye, Metal-free carbon materials for persulfate-based advanced oxidation process: microstructure, property and tailoring, *Prog. Mater. Sci.*, 111 (2020) 100654, doi: 10.1016/j.pmatsci.2020.100654.
- [14] Y. Li, R. Baghi, J. Filip, S. Islam, L. Hope-weeks, W.L. Yan, Activation of peroxydisulfate by ferrite materials for phenol degradation, *ACS Sustainable Chem. Eng.*, 7 (2019) 8099–8108.
- [15] G.Y. Chen, G.Y. Wu, N. Li, X.K. Lu, J.H. Zhao, M.T. He, B.B. Yan, H.Q. Zhang, X.G. Duan, S.B. Wang, Landfill leachate treatment by persulfate related advanced oxidation technologies, *J. Hazard. Mater.*, 418 (2021) 126355, doi: 10.1016/j.jhazmat.2021.126355.
- [16] S.H. Chen, L.Y. Ma, Y.G. Du, W. Zhan, T.C. Zhang, D.Y. Du, Highly efficient degradation of rhodamine B by carbon nanotubes-activated persulfate, *Sep. Purif. Technol.*, 256 (2021) 117788, doi: 10.1016/j.seppur.2020.117788.
- [17] X.W. Ao, W.J. Liu, W.J. Sun, M.Q. Cai, C. Yang, Z.D. Lu, C. Li, Medium pressure UV-activated peroxymonosulfate for ciprofloxacin degradation: kinetics, mechanism, and genotoxicity, *Chem. Eng. J.*, 345 (2018) 87–97.
- [18] M.M. Zhang, Y. Gong, N. Ma, X. Zhao, Promoted photoelectrocatalytic degradation of BPA with peroxymonosulfate on a  $\text{MnFe}_2\text{O}_4$  modified carbon paper cathode, *Chem. Eng. J.*, 399 (2020) 125088, doi: 10.1016/j.cej.2020.125088.
- [19] X.Q. Zhou, A. Jawad, M.Y. Luo, C.G. Luo, T.T. Zhang, H.B. Wang, J. Wang, S.L. Wang, Z.L. Chen, Z.Q. Chen, Regulating activation pathway of Cu/persulfate through the incorporation of unreducible metal oxides: pivotal role of surface oxygen vacancies, *Appl. Catal., B*, 286 (2021) 119914, doi: 10.1016/j.apcatb.2021.119914.
- [20] G.D. Fang, W.H. Wu, Y.M. Deng, D.W. Zhou, Homogenous activation of persulfate by different species of vanadium ions for PCBs degradation, *Chem. Eng. J.*, 323 (2017) 84–95.
- [21] X.L. Zhang, M.B. Feng, R.J. Qu, H. Liu, L.S. Wang, Z.Y. Wang, Catalytic degradation of diethyl phthalate in aqueous solution by persulfate activated with nano-scaled magnetic  $\text{CuFe}_2\text{O}_4/\text{MWCNTs}$ , *Chem. Eng. J.*, 301 (2016) 1–11.
- [22] J.L. Wang, S.C. Wang, Activation of persulfate (PS) and peroxymonosulfate (PMS) and application for the degradation of emerging contaminants, *Chem. Eng. J.*, 334 (2018) 1502–1517.
- [23] T. Dippong, E.A. Levei, O. Cadar, Recent advances in synthesis and applications of  $\text{MFe}_2\text{O}_4$  (M = Co, Cu, Mn, Ni, Zn) nanoparticles, *Nanomaterials*, 11 (2021) 1560, doi: 10.3390/nano11061560.
- [24] J. Li, J.F. Yan, G. Yao, Y.H. Zhang, X. Li, B. Lai, Improving the degradation of atrazine in the three-dimensional (3D) electrochemical process using  $\text{CuFe}_2\text{O}_4$  as both particle electrode and catalyst for persulfate activation, *Chem. Eng. J.*, 361 (2019) 1317–1332.
- [25] K. Guan, P.J. Zhou, J.Y. Zhang, L.L. Zhu, Catalytic degradation of Acid Orange 7 in water by persulfate activated with  $\text{CuFe}_2\text{O}_4@ \text{RSDBC}$ , *Mater. Res. Express*, 7 (2020) 016529.
- [26] B.Y. Wang, Q.Q. Li, Y. Lv, H.B. Fu, D.Y. Liu, Y.F. Feng, H.F. Xie, H.X. Qu, Insights into the mechanism of peroxydisulfate activated by magnetic spinel  $\text{CuFe}_2\text{O}_4/\text{SBC}$  as a heterogeneous catalyst for bisphenol S degradation, *Chem. Eng. J.*, 416 (2021) 129162, doi: 10.1016/j.cej.2021.129162.
- [27] W.X. Qin, G.D. Fang, Y.J. Wang, D.M. Zhou, Mechanistic understanding of polychlorinated biphenyls degradation by peroxymonosulfate activated with  $\text{CuFe}_2\text{O}_4$  nanoparticles: key role of superoxide radicals, *Chem. Eng. J.*, 348 (2018) 526–534.
- [28] H.X. Zhang, Y.Y. Song, L.C. Nengzi, J.F. Gou, B. Li, X.W. Chen, Activation of persulfate by a novel magnetic  $\text{CuFe}_2\text{O}_4/\text{Bi}_2\text{O}_3$  composite for lomefloxacin degradation, *Chem. Eng. J.*, 379 (2020) 122362, doi: 10.1016/j.cej.2019.122362.
- [29] H. Lee, H.J. Lee, J. Jeong, J. Lee, N.B. Park, C. Lee, Activation of persulfates by carbon nanotubes: oxidation of organic compounds by nonradical mechanism, *Chem. Eng. J.*, 266 (2015) 28–33.
- [30] T. Zhang, Y. Chen, Y.R. Wang, J. Le Roux, Y. Yang, J. Croué, Efficient peroxydisulfate activation process not relying on sulfate radical generation for water pollutant degradation, *Environ. Sci. Technol.*, 48 (2014) 5868–5875.
- [31] Y. Feng, C.Z. Liao, L.J. Kong, D.L. Wu, Y.M. Liu, P.H. Lee, K. Shih, Facile synthesis of highly reactive and stable Fe-doped  $\text{g-C}_3\text{N}_4$  composites for peroxymonosulfate activation: a novel nonradical oxidation process, *J. Hazard. Mater.*, 354 (2018) 63–71.
- [32] X. Chen, W.D. Oh, T.T. Lim, Graphene- and CNTs-based cocatalysts in persulfates activation: material design and catalytic mechanisms, *Chem. Eng. J.*, 354 (2018) 941–976.
- [33] P.F. Xiao, L. An, D.D. Wu, The use of carbon materials in persulfate-based advanced oxidation processes: a review, *New Carbon Mater.*, 35 (2020) 667–683.
- [34] A. Jawad, J. Lang, Z.W. Liao, A. Khan, J. Ifthikar, Z.A. Lv, A.J. Long, Z.L. Chen, Z.Q. Chen, Activation of persulfate by  $\text{CuO}_x/\text{Co-LDH}$ : a novel heterogeneous system for contaminant degradation with broad pH window and controlled leaching, *Chem. Eng. J.*, 335 (2018) 548–559.

- [35] X.G. Duan, H.Q. Sun, M. Tade, S.B. Wang, Metal-free activation of persulfate by cubic mesoporous carbons for catalytic oxidation via radical and nonradical processes, *Catal. Today*, 307 (2018) 140–146.
- [36] X.H. Ren, H.H. Guo, J.K. Feng, P.C. Si, L. Zhang, L.J. Ci, Synergistic mechanism of adsorption and metal-free catalysis for phenol degradation by N-doped graphene aerogel, *Chemosphere*, 191 (2018) 389–399.
- [37] P.F. Xue, J. Gao, Y.B. Bao, J.B. Wang, Q.Y. Li, C.F. Wu, An analysis of microstructural variations in carbon black modified by oxidation or ultrasound, *Carbon*, 49 (2011) 3346–3355.
- [38] M.A. Fayidh, S. Kallary, P.A.S. Babu, M. Sivarajan, M. Sukumar, A rapid and miniaturized method for the selection of microbial phenol degraders using colourimetric microtitration, *Curr. Microbiol.*, 70 (2015) 898–906.
- [39] Environmental Protection Industry Standard HJ/T 399-2007, Water Quality-Determination of the Chemical Oxygen Demand-Fast Digestion-Spectrophotometric Method, Ministry of Ecology and Environment of the People's Republic of China, 2007.
- [40] C.J. Liang, C.F. Huang, N.H. Mohanty, R.M. Kurakalva, A rapid spectrophotometric determination of persulfate anion in ISCO, *Chemosphere*, 73 (2008) 1540–1543.
- [41] H.X. Zhang, Y.Y. Song, L.C. Nengzi, J.F. Gou, B. Li, X.W. Cheng, Activation of persulfate by a novel magnetic  $\text{CuFe}_2\text{O}_4/\text{Bi}_2\text{O}_3$  composite for lomefloxacin degradation, *Chem. Eng. J.*, 379 (2020) 122362, doi: 10.1016/j.cej.2019.122362.
- [42] J. Li, Y. Ren, F.Z. Ji, B. Lai, Heterogeneous catalytic oxidation for the degradation of p-nitrophenol in aqueous solution by persulfate activated with  $\text{CuFe}_2\text{O}_4$  magnetic nano-particles, *Chem. Eng. J.*, 324 (2017) 63–73.
- [43] P.C. Guo, H.B. Qiu, C.W. Yang, X. Zhang, X.Y. Shai, Y.L. Lai, G.P. Sheng, Highly efficient removal and detoxification of phenolic compounds using persulfate activated by  $\text{MnOx}@\text{OMC}$ : synergistic mechanism and kinetic analysis, *J. Hazard. Mater.*, 402 (2021) 123846, doi: 10.1016/j.jhazmat.2020.123846.
- [44] J. Romanos, M. Beckner, D. Stalla, A. Tekeci, G. Suppes, S. Jalisatgi, M. Lee, F. Hawthorne, J.D. Robertson, L. Fielej, B. Kuchta, C. Wexler, P. Yu, P. Pfeifer, Infrared study of boron-carbon chemical bonds in boron-doped activated carbon, *Carbon*, 54 (2013) 208–214.
- [45] A.Q. Chen, S.J. Xia, Z.G. Ji, H.W. Lu, Insights into the origin of super-high oxygen evolution potential of Cu doped  $\text{SnO}_2$  anodes: a theoretical study, *Appl. Surf. Sci.*, 471 (2019) 149–153.
- [46] M. Moradi, Y. Vasseghian, A. Khataee, M. Harati, H. Arfaeinia, Ultrasound-assisted synthesis of  $\text{FeTiO}_3/\text{GO}$  nanocomposite for photocatalytic degradation of phenol under visible light irradiation, *Sep. Purif. Technol.*, 261 (2021) 118274, doi: 10.1016/j.seppur.2020.118274.
- [47] Rahmi, Lelifajri, R. Nurfatimah, Preparation of polyethylene glycol diglycidyl ether (PEDGE) crosslinked chitosan/activated carbon composite film for  $\text{Cd}^{2+}$  removal, *Carbohydr. Polym.*, 199 (2018) 499–505.
- [48] L.P. Fang, K. Liu, F.B. Li, W.B. Zeng, Z.B. Hong, L. Xu, Q.T. Shi, Y.B. Ma, New insights into stoichiometric efficiency and synergistic mechanism of persulfate activation by zero-valent bimetal (Iron/Copper) for organic pollutant degradation, *J. Hazard. Mater.*, 403 (2021) 123669, doi: 10.1016/j.jhazmat.2020.123669.
- [49] J. Wang, X.Y. Xu, Q.J. Zhong, Z.B. Xu, L. Zhao, H. Qiu, X.D. Gao, Roles of the mineral constituents in sludge-derived biochar in persulfate activation for phenol degradation, *J. Hazard. Mater.*, 398 (2020) 122861, doi: 10.1016/j.jhazmat.2020.122861.
- [50] C. Li, V. Goetz, S. Chiron, Peroxydisulfate activation process on copper oxide:  $\text{Cu(III)}$  as the predominant selective intermediate oxidant for phenol and waterborne antibiotics removal, *J. Environ. Chem. Eng.*, 9 (2021) 105145, doi: 10.1016/j.jece.2021.105145.
- [51] W.C. Yang, X.M. Li, D.D. Xi, Q. Li, Z.H. Yang, X.B. Min, Synergistic chromium(VI) reduction and phenol oxidative degradation by  $\text{FeS}_2/\text{Fe}^0$  and persulfate, *Chemosphere*, 281 (2021) 130957, doi: 10.1016/j.chemosphere.2021.130957.
- [52] Y. Zhao, M. Song, Q. Cao, P.Z. Sun, Y.H. Chen, F.Y. Meng, The superoxide radicals' production via persulfate activated with  $\text{CuFe}_2\text{O}_4$ @biochar composites to promote the redox pairs cycling for efficient degradation of o-nitrochlorobenzene in soil, *J. Hazard. Mater.*, 400 (2020) 122887, doi: 10.1016/j.jhazmat.2020.122887.
- [53] C.D. Qi, X.T. Liu, J. Ma, C.Y. Lin, X.W. Li, H.J. Zhang, Activation of peroxymonosulfate by base: implications for the degradation of organic pollutants, *Chemosphere*, 151 (2016) 280–288.
- [54] S. Madihi-Bidgoli, S. Asadnezhad, A. Yaghoot-Nezhad, A. Hassani, Azurobine degradation using  $\text{Fe}_2\text{O}_3$ @multi-walled carbon nanotube activated peroxymonosulfate (PMS) under UVA-LED irradiation: performance, mechanism and environmental application, *J. Environ. Chem. Eng.*, 9 (2021) 106660, doi: 10.1016/j.jece.2021.106660.
- [55] L.D. Lai, J.F. Yan, J. Li and B. Lai,  $\text{Co/Al}_2\text{O}_3$ -EPM as peroxymonosulfate activator for sulfamethoxazole removal: performance, biotoxicity, degradation pathways and mechanism, *Chem. Eng. J.*, 343 (2018) 676–688.
- [56] X.J. Li, F.Z. Liao, L.M. Ye, L.Z. Yeh, Controlled pyrolysis of MIL-88A to prepare iron/carbon composites for synergistic persulfate oxidation of phenol: catalytic performance and mechanism, *J. Hazard. Mater.*, 398 (2020) 122938, doi: 10.1016/j.jhazmat.2020.122938.
- [57] J.B. Peng, Z.X. Wang, S.Y. Wang, J. Liu, Y.Z. Zhang, B.J. Wang, Z.M. Gong, M.J. Wang, H. Dong, J.L. Shi, H.J. Liu, G.X. Yan, G.G. Liu, S.X. Gao, Z.G. Cao, Enhanced removal of methylparaben mediated by cobalt/carbon nanotubes ( $\text{Co/CNTs}$ ) activated peroxymonosulfate in chloride-containing water: reaction kinetics, mechanisms and pathways, *Chem. Eng. J.*, 409 (2021) 128176, doi: 10.1016/j.cej.2020.128176.
- [58] X.W. Huo, P. Zhou, J. Zhang, Y.X. Liu, X. Cheng, Y. Liu, W.S. Li, Y.L. Zhang, N, S-Doped porous carbons for persulfate activation to remove tetracycline: nonradical mechanism, *J. Hazard. Mater.*, 391 (2020) 122055, doi: 10.1016/j.jhazmat.2020.122055.
- [59] Z.N. Tu, Y.M. Qi, R.J. Qu, X.S. Tang, Z.Y. Wang, Z.L. Huo, Photochemical transformation of hexachlorobenzene (HCB) in solid-water system: kinetics, mechanism and toxicity evaluation, *Chemosphere*, 295 (2022) 133907, doi: 10.1016/j.chemosphere.2022.133907.
- [60] J.C. Lyu, M. Ge, Z. Hu, C.S. Guo, One-pot synthesis of magnetic  $\text{CuO/Fe}_2\text{O}_3/\text{CuFe}_2\text{O}_4$  nanocomposite to activate persulfate for levofloxacin removal: Investigation of efficiency, mechanism and degradation route, *Chem. Eng. J.*, 389 (2020) 4055–4067.
- [61] Y.W. Shi, J.D. Zhu, H.W. Zhang, Activation of persulfate by EDTA-2K-derived nitrogen-doped porous carbons for organic contaminant removal: radical and non-radical pathways, *Chem. Eng. J.*, 386 (2020) 124009, doi: 10.1016/j.cej.2019.124009.
- [62] T. Zhang, H.B. Zhu, J.P. Croue, Production of sulfate radical from peroxymonosulfate induced by a magnetically separable  $\text{CuFe}_2\text{O}_4$  spinel in water: efficiency, stability, and mechanism, *Environ. Sci. Technol.*, 47 (2013) 2784–2791.
- [63] Z.L. Li, C.S. Guo, J.C. Lyu, Z. Hu, M. Ge, Tetracycline degradation by persulfate activated with magnetic  $\text{Cu/CuFe}_2\text{O}_4$  composite: efficiency, stability, mechanism and degradation pathway, *J. Hazard. Mater.*, 373 (2019) 85–96.
- [64] X. Cheng, H.G. Guo, Y.L. Zhang, G.V. Korshin, B. Yang, Insights into the mechanism of nonradical reactions of persulfate activated by carbon nanotubes: activation performance and structure-function relationship, *Water Res.*, 157 (2019) 406–414.
- [65] H. Zhang, Y. Liu, F. Jiang, X. Bai, H.J. Li, D. Lang, L. Wang, B. Pan, Persulfate adsorption and activation by carbon structure defects provided new insights into ofloxacin degradation by biochar, *Sci. Total. Environ.*, 806 (2022) 150968, doi: 10.1016/j.scitotenv.2021.150968.